

Hybridization between surface flat bands and bulk bands in the topological nodal-line semimetal $\text{Sn}_{0.15}\text{NbSe}_{1.75}$ probed via soft-point-contact spectroscopy

K. Kumarasinghe,¹ C. Dissanayake,¹ R. Munir,¹ M. Tomlinson,¹ and Y. Nakajima^{1,*}

¹*Department of Physics, University of Central Florida, Orlando, Florida 32816, USA*

(Dated: January 17, 2025)

We report a detailed study of soft-point-contact spectroscopy of the superconducting topological nodal-line semimetal $\text{Sn}_{0.15}\text{NbSe}_{1.75}$ with the superconducting transition temperature $T_c = 9.5$ K. In the normal state, we observe prominent asymmetric double peaks in the differential conductance dI/dV . The asymmetric dI/dV curves are attributed to Fano resonance, quantum interference between two distinct tunneling paths of transmitting electrons into flat energy bands and dispersive bands. A phenomenological double Fano resonance model reveals the hybridization between these bands below the hybridization temperature $T_{\text{hyb}} = 23$ K. This hybridization drives an opening of a pseudogap below a characteristic temperature $T_{\text{PG}} = 6.8$ K. In the superconducting state, we observe an unusual upper critical field that increases linearly with decreasing temperatures from $0.4T_c$ to $0.01T_c$, suggestive of a possible exotic superconducting state. Our results suggest the presence of surface flat energy bands that stem from nontrivial topological nature of nodal lines in the bulk band structure and the hybridization between the surface flat bands and bulk bands in $\text{Sn}_{0.15}\text{NbSe}_{1.75}$.

I. INTRODUCTION

Flat energy band systems represent one of the most exciting frontiers in the current condensed matter physics research. The dispersionless energy bands with the extremely large density of states near Fermi energy cause a plethora of exotic quantum states of matter, including ferromagnetism [1], unconventional superconductivity [2], heavy fermion states [3], fractional quantum Hall states [4], strange metallic states [5], and Mott insulating states [6]. These exotic states can be stabilized in various materials, such as magic-angle twisted bilayer graphene [2, 5–8], moiré transition metal dichalcogenides [9–11], f -electron intermetallics [3], and kagome materials [12–16].

While these materials host flat energy bands in their bulk electronic structures, nondispersive energy bands can also originate from boundaries, i.e., surfaces on materials. A notable system that harbors flat surface energy bands is a topological nodal-line semimetal [17–20]. In topological nodal-line semimetals, the bulk conduction and valence bands intersect in the Brillouin zone, forming closed loops instead of the discrete points found in Dirac and Weyl semimetals. These crossings are nonaccidental or symmetry-protected; thus, they cannot be lifted by perturbations without breaking the underlying symmetries. The topologically stable nodal lines in bulk bands give rise to approximately dispersionless surface states, so-called drumhead surface states, bounded by a projection of the bulk nodal line onto the surface plane. The dispersionless surface states provide a promising platform for the realization of high-

temperature superconductivity [21] as well as topological superconducting states through bulk-surface coupling [22, 23]. Therefore, elucidating the effects of surface-bulk interaction is key to harnessing the topological nature, spin textures, and nondispersive energy bands of surface states in bulk topological nodal-line materials.

One of the promising materials for investigating the exotic phenomena arising from the coupling between nondispersive surface states and bulk states is $\text{Sn}_x\text{NbSe}_{2-\delta}$. This material shares a noncentrosymmetric crystal structure with ABSe_2 ($A = \text{Sn, Pb}$ and $B = \text{Nb, Ta}$) [24, 25] [the inset of FIG.1(a)]. The ABSe_2 family is theoretically predicted to be a topological nodal line semimetal and exhibit superconductivity at low temperatures [26]. In fact, recent studies have experimentally revealed the drumhead surface states associated with topological nodal lines [22, 23, 27] and superconductivity at 3.8 K [22, 28–31] in PbTaSe_2 . According to the theoretical calculations [26], SnNbSe_2 has bulk nodal lines located very close to Fermi energy and shows superconductivity at the highest superconducting transition temperature $T_c = 7$ K. Interestingly, off-stoichiometric $\text{Sn}_x\text{NbSe}_{2-\delta}$ shows unusual superconductivity. Its T_c can be fine-tuned between 5 and 12 K—higher than the predicted value for SnNbSe_2 —as Sn concentration x and Se deficiency δ are controlled [25]. Moreover, the in-plane upper critical field of low T_c samples ($T_c \sim 5$ K) exceeds the BCS Pauli paramagnetic limit by a factor of ~ 2 , suggestive of a possible odd-parity superconducting pairing state [24]. Despite these intriguing findings, the presence of the surface states in $\text{Sn}_{0.15}\text{NbSe}_{1.75}$ remains unproven.

We here report the presence of flat-band surface states and the surface-bulk coupling in the tentative topological nodal-line semimetal $\text{Sn}_{0.15}\text{NbSe}_{1.75}$, probed via

* Corresponding author: Yasuyuki.Nakajima@ucf.edu

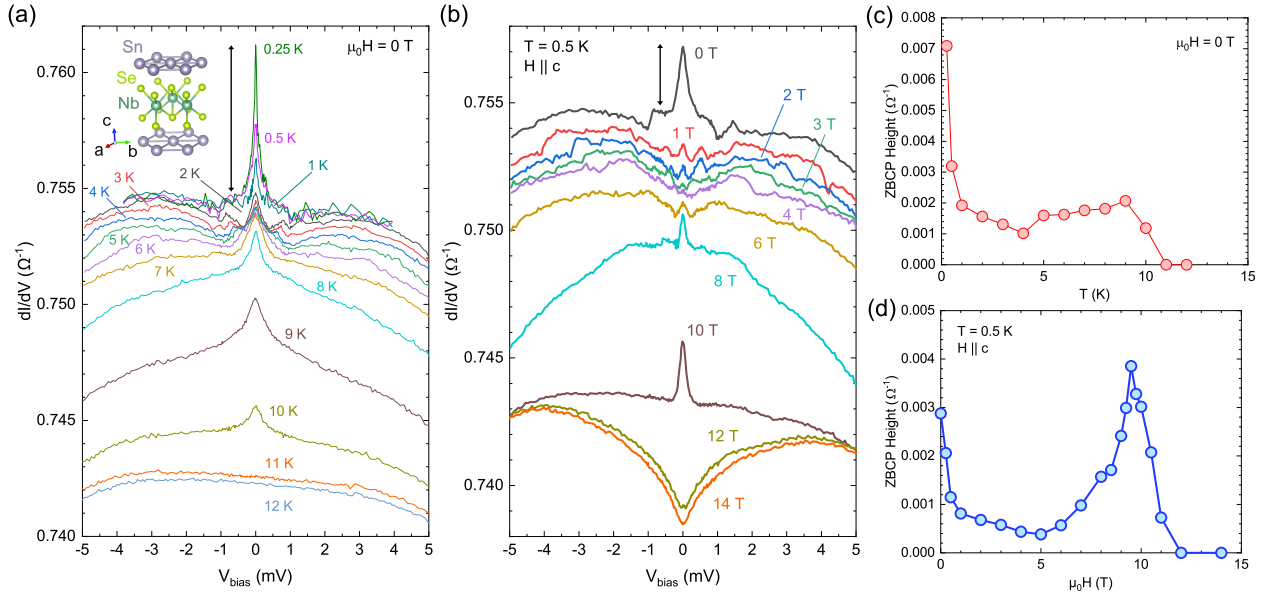


FIG. 1. (a) Differential conductance dI/dV of $\text{Sn}_{0.15}\text{NbSe}_{1.75}$ in zero magnetic field. Inset: noncentrosymmetric crystal structure of SnNbSe_2 . (b) dI/dV at 0.5 K in magnetic fields. Magnetic fields are applied parallel to the c axis. (c) ZBCP height as a function of temperatures in zero magnetic field. The ZBCP height is defined by the double arrow in the panel (a). (d) ZBCP height as a function of the magnetic field at 0.5 K. The ZBCP height is defined by the double arrow in the panel (b).

soft-point-contact spectroscopy. We observe asymmetric double peaks in differential conductance dI/dV in the normal state, suggestive of Fano resonance, the quantum interference between tunneling paths of electrons into discrete and continuous energy states. Exploiting a phenomenological double Fano resonance model, we reveal the hybridization between the flat energy bands and bulk bands. We also observe an opening of a pseudogap in dI/dV . The obtained hybridization gap amplitude Δ_{hyb} is closely correlated with the pseudogap amplitude Δ_{PG} , as observed in the heavy fermion superconductor CeCoIn_5 [32]. In the superconducting state, we find a prominent zero-bias conductance peak (ZBCP) in dI/dV and its unusual temperature and magnetic field dependence. The ZBCP most likely arises from an extrinsic origin. The upper critical field shows linear-in- T behavior at low temperatures down to $0.01T_c$, different from that predicted by the Werthamer-Helfand-Hohenberg (WHH) theory for conventional type-II superconductors. The anomalous temperature dependence of H_{c2} may be suggestive of an unusual superconducting state. Our findings suggest that the presence of surface flat bands, induced by topological nodal lines in the bulk bands, and the hybridization between the surface flat bands and bulk bands in $\text{Sn}_{0.15}\text{NbSe}_{1.75}$.

II. EXPERIMENTAL METHODS

$\text{Sn}_{0.15}\text{NbSe}_{1.75}$ single crystals were grown using a self-flux method [24, 25]. The excess of molten Sn flux was removed by centrifuging. We obtained a single-crystal x-ray diffraction pattern consistent with the noncentrosymmetric crystal structure of SnNbSe_2 with the space group $P\bar{6}m2$ and clearly different from the $2H\text{-NbSe}_2$ -type structure of Sn-intercalated NbSe_2 with Sn concentration up to 0.04. The atomic ratio of the crystal was determined with x-ray fluorescence spectroscopy. Soft-point-contact spectra were obtained by a lock-in technique with ac current modulation [33, 34]. An Au/Ag/ $\text{Sn}_{0.15}\text{NbSe}_{1.75}$ point-contact junction was fabricated using Ag paste on the ab plane of the sample surface. We used a quasi-four-probe configuration to measure the point-contact spectra.

III. RESULTS AND DISCUSSION

In the differential conductance dI/dV of $\text{Sn}_{0.15}\text{NbSe}_{1.75}$, we observe anomalous behavior in both the normal and superconducting states. We plot dI/dV of $\text{Sn}_{0.15}\text{NbSe}_{1.75}$ as a function of bias voltage V_{bias} in zero magnetic field in FIG.1(a). In the normal state at high temperatures above 11 K, dI/dV curves exhibit asymmetric parabola-like shapes. Upon cooling the temperature below 10 K, a peak appears

at $V_{\text{bias}} = 0$, associated with superconductivity. The zero-bias-conductance peak (ZBCP) becomes more prominent and sharper at low temperatures, as manifested in the unusual temperature dependence of ZBCP height shown in FIG.1(c).

Superconductivity of $\text{Sn}_{0.15}\text{NbSe}_{1.75}$ is suppressed by magnetic fields, leading to the emergence of double peaks in the normal state dI/dV . dI/dV of $\text{Sn}_{0.15}\text{NbSe}_{1.75}$ at 0.5 K in applied magnetic fields is plotted as a function of V_{bias} in FIG.1(b). The magnetic fields are applied perpendicular to the ab plane. As the applied magnetic field increases, the ZBCP height is suppressed gradually until reaching $\mu_0 H = 5$ T. With increasing applied magnetic field above 5 T, the ZBCP is enhanced again, becoming particularly pronounced around 10 T in the vicinity of H_{c2} . The anomalous field dependence of the ZBCP is more clearly shown in FIG.1(d). Above $\mu_0 H = 12$ T, the ZBCP disappears, indicating that the superconductivity is completely suppressed. In the normal state above 12 T, notable double peaks around ± 4 mV are observed in dI/dV accompanied by a sharp dip at $V_{\text{bias}} = 0$.

The asymmetry in dI/dV persists even at high magnetic fields, demonstrating its robustness against applied magnetic fields. In contrast, the double peaks in dI/dV diminish as the temperature increases. Figure 2 illustrates the evolution of the double peaks in dI/dV at an applied magnetic field of $\mu_0 H = 14$ T. While the double peaks are prominent at 0.5 K, its amplitudes gradually decrease as the temperature increases.

We observe two distinct anomalous features in dI/dV of $\text{Sn}_{0.15}\text{NbSe}_{1.75}$: 1) the asymmetric double peaks in the normal state and 2) ZBCP in the superconducting state. First, we will discuss the origin of the asymmetric dI/dV in the normal state.

The asymmetric double peaks in dI/dV of $\text{Sn}_{0.15}\text{NbSe}_{1.75}$ are *not* caused by extrinsic non-spectroscopic effect, local heating at a point-contact junction in the thermal regime, where the mean free path ℓ is much shorter than the junction diameter d , $\ell \ll d$ [35]. In the thermal regime, the voltage drop occurs within the junction due to inelastic scattering, yielding local Joule heating. In this situation, the temperature at the point-contact junction, T_J , is given by,

$$T_J^2 = T_0^2 + V_{\text{bias}}^2/4L_0, \quad (1)$$

where T_0 is the bath temperature and $L_0 = (\pi e k_B)^2/3$ is the Lorenz number. Here, we assume that the Wiedemann-Franz law is valid and the Lorenz number is independent of temperature within the measured temperature range. If the junction is in the thermal regime, differential resistance dV/dI as a function of T_J mimics the temperature dependence of the bulk resistivity. To verify this, we plot dV/dI at 0.5 K in an applied field of 14 T as a function of T_J obtained from Eq. (1) in FIG.3.

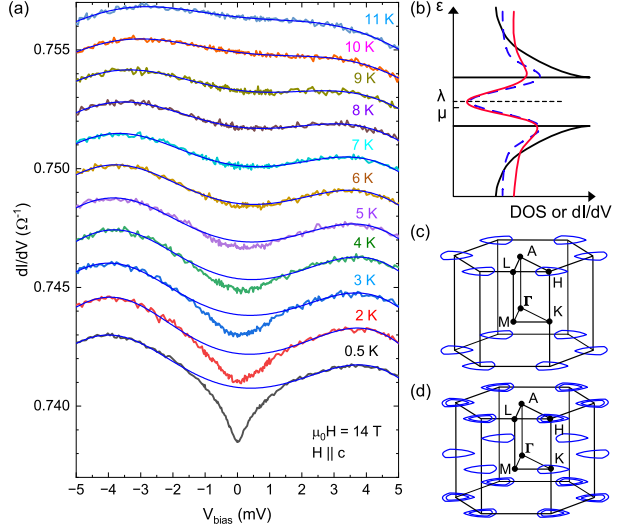


FIG. 2. dI/dV of $\text{Sn}_{0.15}\text{NbSe}_{1.75}$ in an applied magnetic field of 14 T. The magnetic field is applied along the c axis. For clarity, the dI/dV curves are successively shifted upward by $0.0015 \Omega^{-1}$. The blue solid lines are fits to the data using the double Fano resonance model, Eq.(3). (b) Schematic diagrams of density of states (DOS) for renormalized bands due to hybridization (thick line) and DOS broadened by correlation effects (blue dashed line). The red line is the expected dI/dV spectrum with Fano resonance. μ is the chemical potential, and λ is the resonance energy. (c) Schematic nodal lines predicted for ABSe_2 without SOC and (d) with SOC.

The upper curve (open symbols) is derived from the positive bias voltage, while the lower one (filled symbols) is from the negative bias voltage. Both dV/dI curves show a clear upturn at low T_J below ~ 10 K. The upturn behavior observed in both dV/dI is inconsistent with the temperature dependence of bulk resistivity, which exhibits $\rho \propto T^5$, as shown in FIG.3(b). This indicates that the junction of our sample is not in the thermal regime and the asymmetric dI/dV results from an intrinsic origin.

Asymmetric dI/dV can be attributed to Fano resonance, which has been observed in various systems with a localized flat energy band, including heavy fermion compounds [36–43] and kagome magnets [34]. The Fano resonance arises from the quantum interference between two distinct tunneling paths: one tunneling into the localized band and the other into the conduction band. These two paths cause the Fano line shape in dI/dV with a peak centered at the resonance energy, λ , which can be described by the Fano resonance model:

$$G_{\text{FR}}(\varepsilon) = \frac{|q - \varepsilon|^2}{1 + \varepsilon^2}, \quad (2)$$

where $\varepsilon = (eV - \lambda)/\Gamma$, Γ is a broadening parameter, and q is a Fano parameter [44].

However, the Fano line shape alone cannot explain

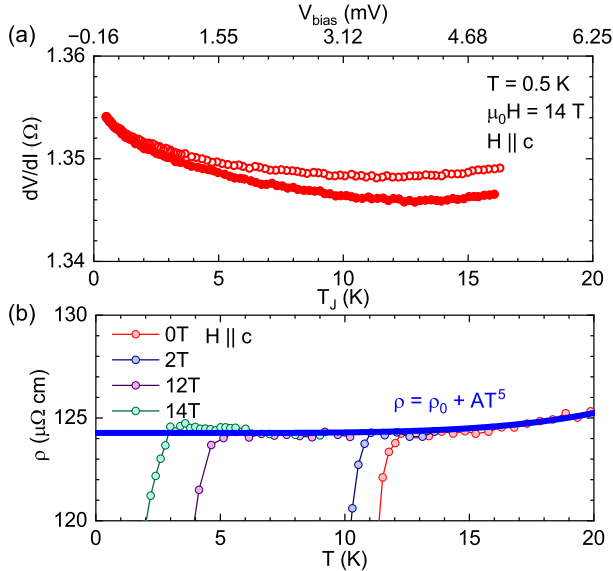


FIG. 3. (a) Differential resistance dV/dI as a function of $T_J = \sqrt{T_0^2 + V_{\text{bias}}^2/4L_0}$. The corresponding V_{bias} is shown on the top axis. (b) Temperature dependence of the resistivity for $\text{Sn}_{0.15}\text{NbSe}_{1.75}$. The blue solid line is a fit to data using $\rho = \rho_0 + AT^5$, suggestive of dominant electron-phonon scattering over electron-electron scattering in the measured temperature range.

the observed double peaks in dI/dV . Similar asymmetric dI/dV with double peaks has indeed been observed in heavy fermion compounds, where Fano resonance is caused by the interference of the tunneling channels into itinerant conduction electrons and localized f electrons [36–43]. In these compounds, the hybridization between the conduction and f electrons induces a hybridization gap. This hybridization gap results in the double peaks and a dip at λ in dI/dV , as illustrated in FIG.2(b). In fact, theoretical models that take into account the hybridization between conduction and f electrons, proposed by Malteva, Dzero, and Coleman (the MDC model) [45] and by Yang (the modified Fano model) [46], successfully reproduce experimental observations in point-contact spectra of heavy fermion system [36–43].

Although Fano resonance requires a localized energy state to interfere with continuous energy states, there are no bulk localized electrons in $\text{Sn}_{0.15}\text{NbSe}_{1.75}$, unlike heavy fermions or kagome materials. Instead, topological nodal-line semimetals, including ABSe_2 , can host dispersionless drumhead surface states associated with nodal lines [17]. In the case of ABSe_2 , nodal lines are located around the H points without spin-orbit coupling (SOC) and additionally around the K points with SOC [26], as shown in FIGs.2 (c) and (d). Enclosed by the projections of these nodal lines onto the surface plane, dispersionless drumhead sur-

face states emerge. While theoretical predictions to off-stoichiometric $\text{Sn}_{0.15}\text{NbSe}_{1.75}$ are currently lacking, we propose that $\text{Sn}_{0.15}\text{NbSe}_{1.75}$ is a topological nodal-line semimetal from analogy to the stoichiometric SnNbSe_2 . In this scenario, we attribute the observed asymmetric double peaks in dI/dV to the interference between two channels into the surface flat bands and bulk bands and the hybridization between these bands.

Since the MDC model and the modified Fano model are primarily proposed for heavy-fermion systems, these models may not be applicable to Fano resonance due to the surface flat bands and the bulk bands in topological nodal-line semimetals. Thus, we fit the data to a phenomenological model that incorporates double Fano lines [41],

$$G_{\text{DFR}}(V) = s[G_{\text{FR}}(\varepsilon_+) + G_{\text{FR}}(\varepsilon_-)] + G_0, \quad (3)$$

where $\varepsilon_{\pm} = (eV - \lambda \pm \Delta/2)/\Gamma$, Δ is the peak separation, s is a scaling factor, and G_0 is a constant background conductance independent of V_{bias} . $G_0 = 0.7348$ is fixed since it remains temperature-independent at 14 T. The obtained parameters Δ , λ , and Γ are plotted in FIG.4. As shown in FIG.2(a), the theoretical curves are in excellent agreement with the experimental dI/dV curves above 7 K. This result reveals two key features in this system: 1) the presence of topological surface flat bands induced by bulk nodal lines and 2) the hybridization between the surface flat bands and bulk bands.

The peak separation Δ is closely linked to the hybridization gap Δ_{hyb} obtained, as reported in the point contact spectroscopy studies of EuNi_2P_2 [41] and UPd_2Al_3 [40]. Temperature dependence of the obtained peak separation, $\Delta(T)$, is plotted in FIG.4 (a). As the temperature increases, the amplitude of $\Delta(T)$ is gradually suppressed. To determine the characteristic temperature T_{hyb} , at which the hybridization gap closes, we fit the data to an empirical expression, $\Delta(T) = \Delta(0)\sqrt{1 - (T/T_{\text{hyb}})^2}$. From this fitting, we obtain $\Delta(0) = 8.37 \pm 0.04$ meV and $T_{\text{hyb}} = 23 \pm 1$ K. According to the previously reported work on the point contact spectroscopy of EuNi_2P_2 , Δ shows similar temperature dependence to Δ_{hyb} obtained from the MDC model and is scaled by a scaling factor $\eta = \Delta/\Delta_{\text{hyb}} = 1.64 \pm 0.03$ [41]. Utilizing this empirical scaling factor η , we obtain $\Delta_{\text{hyb}}(0) = 5.3 \pm 0.1$ meV for $\text{Sn}_{0.15}\text{NbSe}_{1.75}$.

The obtained values of λ and Γ provide insights into the surface flat energy bands. As shown in FIG.4(b), λ for $\text{Sn}_{0.15}\text{NbSe}_{1.75}$ is ~ 0.48 meV and nearly independent of temperature, indicating that the surface flat energy bands are located close to the Fermi energy. The broadening parameter Γ increases with temperatures, varying as $\Gamma(T) = \sqrt{(\alpha k_B T)^2 + 2(k_B T_K)^2}$, the expression describing a single-site Kondo resonance [47]. From the theoretical curve, we extract $\alpha = 4.0 \pm 0.1$ and $T_K = 31.0 \pm 0.4$ K. The obtained value of α is slightly larger than $\alpha = \pi$ for the single-site Kondo model.

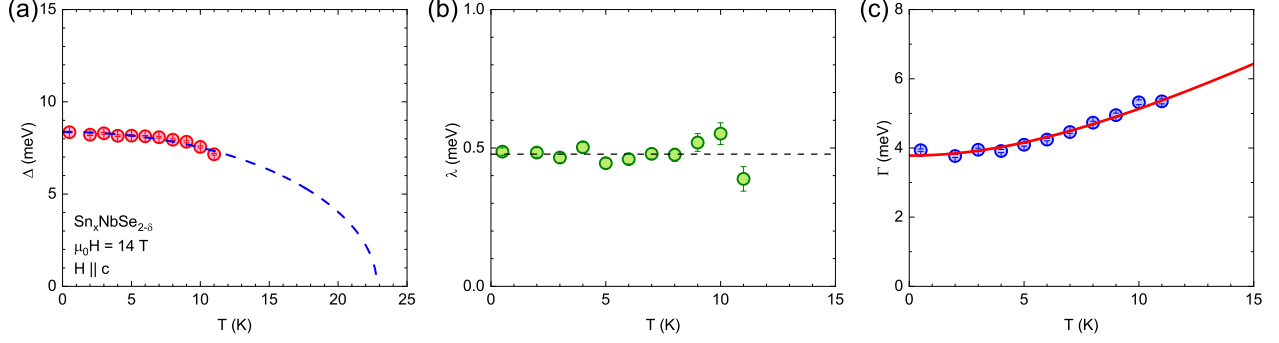


FIG. 4. (a) Temperature dependence of the peak separation Δ . The blue dashed line is a fit to the data using $\Delta(T) = \Delta(0)\sqrt{1 - (T/T_{\text{hyb}})^2}$ with $\Delta(0) = 8.37 \pm 0.04$ meV and $T_{\text{hyb}} = 23 \pm 1$ K. (b) The resonance energy λ as a function of temperature. The black dashed line is the average value of the resonance energy over the measured T range, $\lambda = 0.48$ meV, suggesting that λ is independent of temperature. (c) Temperature dependence of the broadening parameter Γ of $\text{Sn}_{0.15}\text{NbSe}_{1.75}$ obtained from a fitting to Eq. (3) at 14 T. The red solid line is a fit to the data using $\Gamma(T) = \sqrt{(\alpha k_B T)^2 + 2(k_B T_K)^2}$ with $\alpha = 4.0 \pm 0.1$ and $T_K = 31.0 \pm 0.4$ K.

$T_K = 31$ K is also slightly larger than the gap-closing temperature T_{hyb} .

The phenomenological double Fano resonance model excellently explains our dI/dV curves above 7 K at 14 T. This finding suggests the presence of surface flat bands and the hybridization between the surface flat bands and bulk bands. However, at temperatures below 7 K, the measured dI/dV curves show noticeable deviations from the theoretical curves around zero-bias voltage, suggestive of an opening of a pseudogap. To highlight the pseudogap-like dip, we normalize the measured dI/dV curves by $G_{\text{DFR}}(V)$ after fitting the background curves to the double Fano resonance model. The normalized curves are plotted in the FIG.5.

The pseudogap of $\text{Sn}_{0.15}\text{NbSe}_{1.75}$ is correlated with the hybridization gap. We define the pseudogap amplitude $2\Delta_{\text{PG}}$ by the deviation from $(dI/dV)/G_{\text{DFR}} = 1$, as indicated by arrows in FIG.5(a). The temperature dependence of $2\Delta_{\text{PG}}$ is shown in the inset of FIG.5. The red dashed line represents an empirical curve of a gap evolution, $2\Delta_{\text{PG}}(T) = 2\Delta_{\text{PG}}(0)\sqrt{1 - (T/T_{\text{PG}})^2}$ with $2\Delta_{\text{PG}} = 3.4 \pm 0.1$ meV and $T_{\text{PG}} = 6.8 \pm 0.2$ K. The ratio of the pseudogap amplitude to the pseudogap temperature is $2\Delta_{\text{PG}}(0)/k_B T_{\text{PG}} = 5.8 \pm 0.2$, which is in good agreement with $2\Delta_{\text{hyb}}(0)/k_B T_{\text{hyb}} = 5.4 \pm 0.3$. This agreement implies that the hybridization gap and pseudogap are driven by the same mechanism, namely, the hybridization between flat surface bands and bulk bands. In fact, a hybridization-controlled pseudogap state is reported in CeCoIn_5 [32]. Our observation may suggest that the hybridization-driven pseudogap opening is a universal feature in systems with flat energy bands and dispersive energy bands.

We now examine dI/dV in the superconducting state of $\text{Sn}_{0.15}\text{NbSe}_{1.75}$. Figure 6(a) shows normalized differential conductance $(dI/dV)_n =$

$[dI/dV(V)]/[dI/dV(-5 \text{ mV})]$ in zero magnetic field at 0.5 K. We observe clear dips at ± 1 meV in $(dI/dV)_n$, associated with the superconducting gap amplitude $2\Delta_{\text{SC}}$. From this characteristic energy scale, we obtain $2\Delta_{\text{SC}}/k_B T_c = 2.58$. We estimate $T_c = 9.5$ K from the midpoint of the resistive transitions of the point-contact junction at $V_{\text{bias}} = 0$. This value is much smaller than the predicted value of 3.43 for BCS weak-coupling superconductors. This small value of $2\Delta_{\text{SC}}/k_B T_c$ can be ascribed to the multigap superconductivity. While the observed dips are associated with a smaller superconducting gap in a passive band, anomaly associated with a larger superconducting gap in an active band is possibly concealed by the background conductance arising from the double peaks and pseudogap due to the hybridization of the surface flat bands and bulk bands.

The upper critical field of $\text{Sn}_{0.15}\text{NbSe}_{1.75}$ shows anomalous temperature dependence at low T . The upper critical field H_{c2} parallel to the c axis is plotted in FIG.6(b), along with theoretical curves calculated using the WHH model. We observe an apparent deviation from a WHH curve with the Maki parameter $\alpha_M = 0$ and the spin-orbit scattering parameter $\lambda_{\text{SO}} = 0$ at low temperatures below 6.5 K $\sim 0.7T_c$, suggestive of the suppression of H_{c2} due to paramagnetic effect. To take the paramagnetic effect into account, we evaluate the Maki parameter using $\alpha_M = \sqrt{2}H_{c2}^{\text{orb}}/H_P = 0.88$, where H_{c2}^{orb} is the orbital limit for dirty superconductors determined by $\mu_0 H_{c2}^{\text{orb}} = -0.69 T_c d(\mu_0 H_{c2})/dT|_{T=T_c} = 11.0$ T and H_P is the BCS Pauli paramagnetic limit, $\mu_0 H_P = 1.86 T_c = 17.7$ T. Using this value and $\lambda_{\text{SO}} = 1.1$, a theoretical curve accurately describes the measured H_{c2} above $T = 2$ K $\sim 0.2T_c$. However, in contrast to the theoretical curves, the measured H_{c2} increases linearly with decreasing temperature from 4 K $\sim 0.4T_c$ to 0.1 K $\sim 0.01T_c$. We note that the simple the-

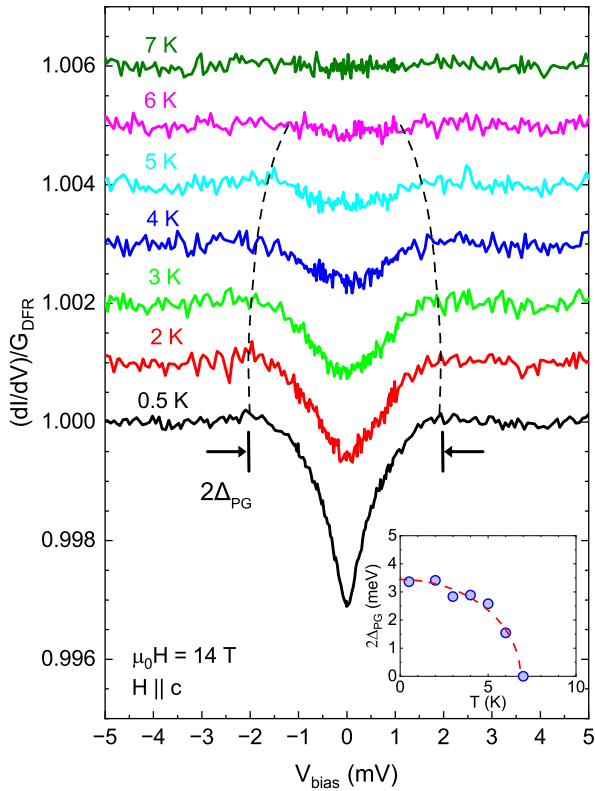


FIG. 5. Normalized differential conductance $(dI/dV)/G_{\text{DFR}}$ of $\text{Sn}_{0.15}\text{NbSe}_{1.75}$ in an applied magnetic field of 14 T. The magnetic field is applied parallel to the c axis. The normalized curves are successively shifted upward by 0.001 for clarity. The pseudogap amplitude $2\Delta_{\text{PG}}$ is defined by the pseudogap width indicated by the arrows. Dashed lines are guides to the eyes. Inset: temperature dependence of $2\Delta_{\text{PG}}$. The red dashed line is a fit to the data using $2\Delta_{\text{PG}}(T) = 2\Delta_{\text{PG}}(0)\sqrt{1 - (T/T_{\text{PG}})^2}$ with $2\Delta_{\text{PG}}(0) = 3.4 \pm 0.1$ meV.

oretical model for H_{c2} of dirty two-gap superconductors [48] cannot reproduce linear-in- T behavior of H_{c2} observed in $\text{Sn}_{0.15}\text{NbSe}_{1.75}$. The anomalous temperature dependence of H_{c2} observed in $\text{Sn}_{0.15}\text{NbSe}_{1.75}$ is reminiscent of those for the iron based superconductors $\text{CaKFe}_4\text{As}_4$ [49] and FeSe [50], in which a Fulde-Ferrell-Larkin-Ovchinnikov state, a pairing state formed between the Zeeman-split Fermi surfaces, is proposed to be stabilized. Although further experimental and theoretical studies, such as using a model taking account of Fermi surface shapes [51], would be required, the linear-in- T behavior of H_{c2} down to $0.01T_c$ may suggest the realization of an exotic superconducting pairing state owing to spin-split Fermi surfaces due to asymmetric SOC in $\text{Sn}_{0.15}\text{NbSe}_{1.75}$.

Finally, we discuss peculiar features of dI/dV in the superconducting state of $\text{Sn}_{0.15}\text{NbSe}_{1.75}$. We observe the prominent ZBCP at low temperatures, as shown in FIG.1(a)) and its unusual temperature and field depen-

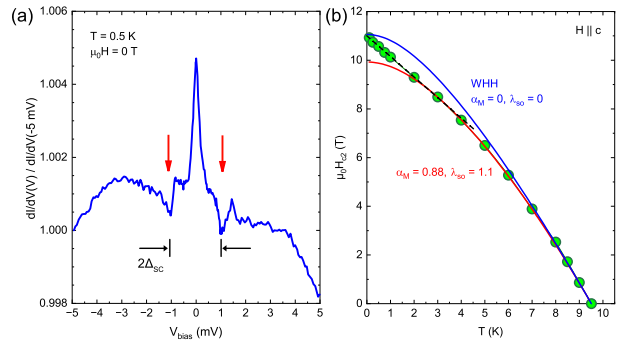


FIG. 6. (a) Normalized differential conductance $(dI/dV)_n = [dI/dV(V)]/[dI/dV(-5 \text{ mV})]$ of $\text{Sn}_{0.15}\text{NbSe}_{1.75}$ at 0.5 K in zero magnetic field. The red arrows indicate dip features associated with the superconducting gap amplitude $2\Delta_{\text{SC}}$. (b) Temperature dependence of upper critical field along the c axis, obtained from the midpoint of resistive transitions in the point-contact junction at $V_{\text{bias}} = 0$. The blue solid line is a theoretical curve based on the WHH theory with $\alpha_{\text{M}} = 0$ and $\lambda_{\text{SO}} = 0$ and the red solid line is a theoretical curve with $\alpha_{\text{M}} = 0.88$ and $\lambda_{\text{SO}} = 1.1$. The black dashed line is a guide to the eyes.

dence, as shown in FIGs.1(c) and (d). A ZBCP can appear in unconventional superconductors with nodes in the gap structure [52, 53] and topological superconductors hosting Majorana zero modes at the surface [54]. However, the extrinsic effect obscures potential intrinsic ZBCPs in our sample. The observed ZBCP at low magnetic fields can arise from the Josephson junction effect between superconducting domains [55, 56], given that the superconducting volume fractions of our $\text{Sn}_{0.15}\text{NbSe}_{1.75}$ single crystals are relatively small. The unusual enhancement of the ZBCP near T_c and H_{c2} can also be attributed to this effect. Indeed, similar enhancement due to the Josephson junction effect has been reported in the point contact spectroscopy of an $\text{La}_{0.9}\text{Ce}_{0.1}\text{CuO}_4$ film [57]. Further experimental efforts are required to clarify the presence of intrinsic ZBCPs in $\text{Sn}_{0.15}\text{NbSe}_{1.75}$.

IV. SUMMARY

In summary, we have studied the normal and superconducting states of $\text{Sn}_{0.15}\text{NbSe}_{1.75}$ using soft-point-contact spectroscopy. Prominent asymmetric double peaks are observed in dI/dV of the normal state. A phenomenological double Fano resonance model can explain the asymmetric double peaks. Our observations uncover the presence of flat energy bands and the hybridization between these flat energy and bulk bands in $\text{Sn}_{0.15}\text{NbSe}_{1.75}$. We also observe a dip feature in dI/dV around $V_{\text{bias}} = 0$ in the normal state due to an opening of a pseudogap. The ratio of the gap ampli-

tude to the gap-closing temperature for the hybridization gap, $2\Delta_{\text{hyb}}(0)/k_{\text{B}}T_{\text{hyb}}$, agree with that for the pseudogap, $2\Delta_{\text{PG}}(0)/k_{\text{B}}T_{\text{PG}}$, suggestive of a hybridization-driven pseudogap. In the superconducting state of $\text{Sn}_{0.15}\text{NbSe}_{1.75}$, a remarkable ZBCP emerges, characterized by unexpected temperature and magnetic field dependencies. However, the ZBCP likely originates from extrinsic effect. Furthermore, the out-of-plane upper critical field displays a linear-in- T behavior at low temperatures down to $0.01T_c$, significantly diverging from the theoretical curves calculated by the WHH theory. This unusual behavior may suggest a possible exotic superconducting state associated with spin-split Fermi

surfaces in $\text{Sn}_{0.15}\text{NbSe}_{1.75}$. Our findings suggest that $\text{Sn}_{0.15}\text{NbSe}_{1.75}$ host topological surface flat bands arising from bulk nodal lines near its Fermi energy and the hybridization between the topological surface flat bands and bulk conduction bands causes the opening of the pseudogap.

ACKNOWLEDGMENTS

The authors thank G. He, K. Jin, Y. Kasahara, and T. Shibauchi for useful discussions. This work was supported by an NSF Career DMR-1944975.

-
- [1] H. Tasaki, From Nagaoka's Ferromagnetism to Flat-Band Ferromagnetism and Beyond: An Introduction to Ferromagnetism in the Hubbard Model, *Prog. Theor. Phys.* **99**, 489 (1998).
- [2] Y. Cao, V. Fatemi, S. Fang, K. Watanabe, T. Taniguchi, E. Kaxiras, and P. Jarillo-Herrero, Unconventional superconductivity in magic-angle graphene superlattices, *Nature* **556**, 43 (2018).
- [3] G. Stewart, Heavy-fermion systems, *Rev. Mod. Phys.* **56**, 755 (1984).
- [4] E. Tang, J.-W. Mei, and X.-G. Wen, High-Temperature Fractional Quantum Hall States, *Phys. Rev. Lett.* **106**, 236802 (2011).
- [5] Y. Cao, D. Chowdhury, D. Rodan-Legrain, O. Rubies-Bigorda, K. Watanabe, T. Taniguchi, T. Senthil, and P. Jarillo-Herrero, Strange Metal in Magic-Angle Graphene with near Planckian Dissipation, *Phys. Rev. Lett.* **124**, 076801 (2020).
- [6] Y. Cao, V. Fatemi, A. Demir, S. Fang, S. L. Tomarken, J. Y. Luo, J. D. Sanchez-Yamagishi, K. Watanabe, T. Taniguchi, E. Kaxiras, R. C. Ashoori, and P. Jarillo-Herrero, Correlated insulator behaviour at half-filling in magic-angle graphene superlattices, *Nature* **556**, 80 (2018).
- [7] I. Das, X. Lu, J. Herzog-Arbeitman, Z.-D. Song, K. Watanabe, T. Taniguchi, B. A. Bernevig, and D. K. Efetov, Symmetry-broken Chern insulators and Rashba-like Landau-level crossings in magic-angle bilayer graphene, *Nat. Phys.* **17**, 710 (2021).
- [8] Y. Xie, A. T. Pierce, J. M. Park, D. E. Parker, E. Khalaf, P. Ledwith, Y. Cao, S. H. Lee, S. Chen, P. R. Forrester, K. Watanabe, T. Taniguchi, A. Vishwanath, P. Jarillo-Herrero, and A. Yacoby, Fractional Chern insulators in magic-angle twisted bilayer graphene, *Nature* **600**, 439 (2021).
- [9] H. Park, J. Cai, E. Anderson, Y. Zhang, J. Zhu, X. Liu, C. Wang, W. Holtzmann, C. Hu, Z. Liu, T. Taniguchi, K. Watanabe, J.-H. Chu, T. Cao, L. Fu, W. Yao, C.-Z. Chang, D. Cobden, D. Xiao, and X. Xu, Observation of fractionally quantized anomalous Hall effect, *Nature* **622**, 74 (2023).
- [10] Y. Zeng, Z. Xia, K. Kang, J. Zhu, P. Knüppel, C. Vaswani, K. Watanabe, T. Taniguchi, K. F. Mak, and J. Shan, Thermodynamic evidence of fractional Chern insulator in moiré MoTe_2 , *Nature* **622**, 69 (2023).
- [11] J. Cai, E. Anderson, C. Wang, X. Zhang, X. Liu, W. Holtzmann, Y. Zhang, F. Fan, T. Taniguchi, K. Watanabe, Y. Ran, T. Cao, L. Fu, D. Xiao, W. Yao, and X. Xu, Signatures of fractional quantum anomalous Hall states in twisted MoTe_2 , *Nature* **622**, 63 (2023).
- [12] Z. Li, J. Zhuang, L. Wang, H. Feng, Q. Gao, X. Xu, W. Hao, X. Wang, C. Zhang, K. Wu, S. X. Dou, L. Chen, Z. Hu, and Y. Du, Realization of flat band with possible nontrivial topology in electronic Kagome lattice, *Sci. Adv.* **4**, eaau4511 (2018).
- [13] J.-X. Yin, S. S. Zhang, G. Chang, Q. Wang, S. S. Tsirkin, Z. Guguchia, B. Lian, H. Zhou, K. Jiang, I. Belopolski, N. Shumiya, D. Multer, M. Litskevich, T. A. Cochran, H. Lin, Z. Wang, T. Neupert, S. Jia, H. Lei, and M. Z. Hasan, Negative flat band magnetism in a spin-orbit-coupled correlated kagome magnet, *Nat. Phys.* **15**, 443 (2019).
- [14] M. Kang, S. Fang, L. Ye, H. C. Po, J. Denlinger, C. Jozwiak, A. Bostwick, E. Rotenberg, E. Kaxiras, J. G. Checkelsky, and R. Comin, Topological flat bands in frustrated kagome lattice CoSn , *Nat. Commun.* **11**, 4004 (2020).
- [15] M. Kang, L. Ye, S. Fang, J.-S. You, A. Levitan, M. Han, J. I. Facio, C. Jozwiak, A. Bostwick, E. Rotenberg, M. K. Chan, R. D. McDonald, D. Graf, K. Kaznatcheev, E. Vescovo, D. C. Bell, E. Kaxiras, J. van den Brink, M. Richter, M. Prasad Ghimire, J. G. Checkelsky, and R. Comin, Dirac fermions and flat bands in the ideal kagome metal FeSn , *Nat. Mater.* **19**, 163 (2020).
- [16] L. Ye, S. Fang, M. Kang, J. Kaufmann, Y. Lee, C. John, P. M. Neves, S. Y. F. Zhao, J. Denlinger, C. Jozwiak, A. Bostwick, E. Rotenberg, E. Kaxiras, D. C. Bell, O. Janson, R. Comin, and J. G. Checkelsky, Hopping frustration-induced flat band and strange metallicity in a kagome metal, *Nat. Phys.* **20**, 610 (2024).
- [17] A. A. Burkov, M. D. Hook, and L. Balents, Topological nodal semimetals, *Phys. Rev. B* **84**, 235126 (2011).
- [18] R. Yu, H. Weng, Z. Fang, X. Dai, and X. Hu, Topological Node-Line Semimetal and Dirac Semimetal State in Antiperovskite Cu_3PdN ,

- Phys. Rev. Lett.* **115**, 036807 (2015).
- [19] H. Weng, Y. Liang, Q. Xu, R. Yu, Z. Fang, X. Dai, and Y. Kawazoe, Topological node-line semimetal in three-dimensional graphene networks, *Phys. Rev. B* **92**, 045108 (2015).
- [20] H. Huang, J. Liu, D. Vanderbilt, and W. Duan, Topological nodal-line semimetals in alkaline-earth stannides, germanides, and silicides, *Phys. Rev. B* **93**, 201114 (2016).
- [21] N. B. Kopnin, T. T. Heikkilä, and G. E. Volovik, High-temperature surface superconductivity in topological flat-band systems, *Phys. Rev. B* **83**, 220503 (2011).
- [22] T.-R. Chang, P.-J. Chen, G. Bian, S.-M. Huang, H. Zheng, T. Neupert, R. Sankar, S.-Y. Xu, I. Belopolski, G. Chang, B. Wang, F. Chou, A. Bansil, H.-T. Jeng, H. Lin, and M. Z. Hasan, Topological Dirac surface states and superconducting pairing correlations in PbTaSe₂, *Phys. Rev. B* **93**, 245130 (2016).
- [23] S.-Y. Guan, P.-J. Chen, M.-W. Chu, R. Sankar, F. Chou, H.-T. Jeng, C.-S. Chang, and T.-M. Chuang, Superconducting topological surface states in the noncentrosymmetric bulk superconductor PbTaSe₂, *Sci. Adv.* **2** (2016), 10.1126/sciadv.1600894.
- [24] R. Munir, K. A. M. H. Siddiquee, C. Dissanayake, X. Hu, Y. Takano, E. S. Choi, and Y. Nakajima, Unusual upper critical fields of the topological nodal-line semimetal candidate Sn_xNbSe_{2-δ}, *J. Phys. Condens. Matter* **33**, 23LT01 (2021).
- [25] R. Munir, K. A. M. H. Siddiquee, C. Dissanayake, K. Kumarasinghe, X. Hu, Y. Takano, E. S. Choi, and Y. Nakajima, Unusual superconductivity in the topological nodal-line semimetal candidate Sn_xNbSe_{1-δ}, *J. Phys. Conf. Ser.* **2164**, 012008 (2022).
- [26] P.-J. Chen, T.-R. Chang, and H.-T. Jeng, Ab initio study of the PbTaSe₂-related superconducting topological metals, *Phys. Rev. B* **94**, 165148 (2016).
- [27] G. Bian, T.-R. Chang, R. Sankar, S.-Y. Xu, H. Zheng, T. Neupert, C.-K. Chiu, S.-M. Huang, G. Chang, I. Belopolski, D. S. Sanchez, M. Neupane, N. Alidoust, C. Liu, B. Wang, C.-C. Lee, H.-T. Jeng, C. Zhang, Z. Yuan, S. Jia, A. Bansil, F. Chou, H. Lin, and M. Z. Hasan, Topological nodal-line fermions in spin-orbit metal PbTaSe₂, *Nat. Commun.* **7**, 10556 EP (2016).
- [28] M. N. Ali, Q. D. Gibson, T. Klimczuk, and R. J. Cava, Noncentrosymmetric superconductor with a bulk three-dimensional Dirac cone gapped by strong spin-orbit coupling, *Phys. Rev. B* **89**, 020505 (2014).
- [29] J. Wang, X. Xu, N. Zhou, L. Li, X. Cao, J. Yang, Y. Li, C. Cao, J. Dai, J. Zhang, Z. Shi, B. Chen, and Z. Yang, Upward Curvature of the Upper Critical Field and the V-Shaped Pressure Dependence of T_{cin} in the Noncentrosymmetric Superconductor PbTaSe₂, *J. Supercond. Nov. Magn.* **28**, 3173 (2015).
- [30] C.-L. Zhang, Z. Yuan, G. Bian, S.-Y. Xu, X. Zhang, M. Z. Hasan, and S. Jia, Superconducting properties in single crystals of the topological nodal semimetal PbTaSe₂, *Phys. Rev. B* **93**, 054520 (2016).
- [31] R. Sankar, G. N. Rao, I. P. Muthuselvam, T.-R. Chang, H. T. Jeng, G. S. Murugan, W.-L. Lee, and F. C. Chou, Anisotropic superconducting property studies of single crystal PbTaSe₂, *J. Phys. Condens. Matter* **29**, 095601 (2017).
- [32] H. Jang, V. Thi Anh Hong, J. Kim, X. Lu, and T. Park, Hybridization-Controlled Pseudogap State in the Quantum Critical Superconductor CeCoIn₅, *Phys. Rev. Lett.* **130**, 076301 (2023).
- [33] D. Daghero and R. S. Gonnelli, Probing multi-band superconductivity by point-contact spectroscopy, *Supercond. Sci. Technol.* **23**, 043001 (2010).
- [34] S. Das and G. Sheet, A modular point contact spectroscopy probe for sub-Kelvin applications, *Rev. Sci. Instrum.* **90**, 103903 (2019).
- [35] Y. G. Naidyuk and I. K. Yanson, Point-Contact Spectroscopy, Vol. 145 (Springer Science+Business Media, Inc., New York, 2005).
- [36] W. K. Park, L. H. Greene, J. L. Sarrao, and J. D. Thompson, Andreev reflection at the normal-metal/heavy-fermion superconductor CeCoIn₅ interface, *Phys. Rev. B* **72**, 052509 (2005).
- [37] G. Goll, T. Brugger, M. Marz, S. Kontermann, H. Löhneysen, T. Sayles, and M. Maple, Point-contact spectroscopy on heavy-fermion superconductors, *Physica B* **378-380**, 665 (2006).
- [38] W. K. Park, P. H. Tobash, F. Ronning, E. D. Bauer, J. L. Sarrao, J. D. Thompson, and L. H. Greene, Observation of the Hybridization Gap and Fano Resonance in the Kondo Lattice URu₂Si₂, *Phys. Rev. Lett.* **108**, 246403 (2012).
- [39] X. Zhang, N. P. Butch, P. Syers, S. Ziemak, R. L. Greene, and J. Paglione, Hybridization, Inter-Ion Correlation, and Surface States in the Kondo Insulator SmB₆, *Phys. Rev. X* **3**, 011011 (2013).
- [40] N. K. Jaggi, O. Mehio, M. Dwyer, L. H. Greene, R. E. Baumbach, P. H. Tobash, E. D. Bauer, J. D. Thompson, and W. K. Park, Hybridization gap in the heavy-fermion compound UPd₂Al₃ via quasiparticle scattering spectroscopy, *Phys. Rev. B* **95**, 165123 (2017).
- [41] M. Shiga, I. Maruyama, K. Okimura, T. Harada, T. Takahashi, A. Mitsuda, H. Wada, Y. Inagaki, and T. Kawae, Evolution of lattice coherence in the intermediate-valence heavy-fermion compound EuNi₂P₂ studied by point contact spectroscopy, *Phys. Rev. B* **103**, L041113 (2021).
- [42] L. Yin, L. Che, T. Le, Y. Chen, Y. Zhang, H. Lee, D. Gnida, J. D. Thompson, D. Kaczorowski, and X. Lu, Point-contact spectroscopy of heavy fermion superconductors Ce₂PdIn₈ and Ce₃PdIn₁₁ in comparison with CeCoIn₅, *J. Phys. Condens. Matter* **33**, 205603 (2021).
- [43] M. Shiga, I. Maruyama, A. Mitsuda, H. Wada, and T. Kawae, Electronic density of state in valence fluctuating kondo lattice systems studied by point-contact spectroscopy, *Low Temp. Phys.* **49**, 876 (2023).
- [44] U. Fano, Effects of Configuration Interaction on Intensities and Phase Shifts, *Phys. Rev.* **124**, 1866 (1961).
- [45] M. Maltseva, M. Dzero, and P. Coleman, Electron Cotunneling into a Kondo Lattice, *Phys. Rev. Lett.* **103**, 206402 (2009).
- [46] Y.-f. Yang, Fano effect in the point contact spectroscopy of heavy-electron materials, *Phys. Rev. B* **79**, 241107 (2009).
- [47] K. Nagaoka, T. Jamneala, M. Grobis, and M. F. Crommie, Temperature Dependence of a Single Kondo Impurity, *Phys. Rev. Lett.* **88**, 077205 (2002).

- [48] A. Gurevich, Enhancement of the upper critical field by nonmagnetic impurities in dirty two-gap superconductors, *Phys. Rev. B* **67**, 184515 (2003).
- [49] M. Bristow, W. Knafo, P. Reiss, W. Meier, P. C. Canfield, S. J. Blundell, and A. I. Coldea, Competing pairing interactions responsible for the large upper critical field in a stoichiometric iron-based superconductor $\text{CaKFe}_4\text{As}_4$, *Phys. Rev. B* **101**, 134502 (2020).
- [50] M. Bristow, A. Gower, J. C. A. Prentice, M. D. Watson, Z. Zajicek, S. J. Blundell, A. A. Haghighirad, A. McCollam, and A. I. Coldea, Multiband description of the upper critical field of bulk FeSe , *Phys. Rev. B* **108**, 184507 (2023).
- [51] T. Shibauchi, L. Krusin-Elbaum, Y. Kasahara, Y. Shimono, Y. Matsuda, R. D. McDonald, C. H. Mielke, S. Yonezawa, Z. Hiroi, M. Arai, T. Kita, G. Blatter, and M. Sigrist, Uncommonly high upper critical field of the pyrochlore superconductor KOs_2O_6 below the enhanced paramagnetic limit, *Phys. Rev. B* **74**, 220506 (2006).
- [52] Y. Tanaka and S. Kashiwaya, Theory of Tunneling Spectroscopy of d-Wave Superconductors, *Phys. Rev. Lett.* **74**, 3451 (1995).
- [53] M. Yamashiro, Y. Tanaka, and S. Kashiwaya, Theory of tunneling spectroscopy in superconducting Sr_2RuO_4 , *Phys. Rev. B* **56**, 7847 (1997).
- [54] S. Sasaki, M. Kriener, K. Segawa, K. Yada, Y. Tanaka, M. Sato, and Y. Ando, Topological Superconductivity in $\text{Cu}_x\text{Bi}_2\text{Se}_3$, *Phys. Rev. Lett.* **107**, 217001 (2011).
- [55] P. A. Lee, Effect of Noise on the Current-Voltage Characteristics of a Josephson Junction, *J. Appl. Phys.* **42**, 325 (1971).
- [56] L. Shan, H. J. Tao, H. Gao, Z. Z. Li, Z. A. Ren, G. C. Che, and H. H. Wen, *s*-wave pairing in MgCNi_3 revealed by point contact tunneling, *Phys. Rev. B* **68**, 144510 (2003).
- [57] G. He, Z.-X. Wei, J. Brisbois, Y.-L. Jia, Y.-L. Huang, H.-X. Zhou, S.-L. Ni, A. V. Silhanek, L. Shan, B.-Y. Zhu, J. Yuan, X.-L. Dong, F. Zhou, Z.-X. Zhao, and K. Jin, Distinction between critical current effects and intrinsic anomalies in the point-contact Andreev reflection spectra of unconventional superconductors, *Chin. Phys. B* **27**, 047403 (2018).